Composition-structure-function correlation of Ca/Zn/AlO_x catalysts for the ketonization of acetic acid

Huajuan Ling,[a] Zichun Wang,[a,b] Leizhi Wang,[a] Catherine Stampfl,[c] Dan Wang,[d] Jianfeng Chen,[d] and Jun Huang[a*]

[a] Laboratory for Catalysis Engineering, School of Chemical and Biomolecular Engineering, The University of Sydney, New South Wales 2006, Australia

[b] Department of Engineering, Macquarie University, Sydney, New South Wales 2109, Australia

[c] School of Physics, The University of Sydney, Sydney, New South Wales 2006, Australia

[d] State Key Laboratory of Organic-Inorganic Composites, Beijing University of Chemical Technology, Beijing 100029, China

[*] To whom correspondence should be addressed:

Tel: +61 2 9351 7483

Fax: +61 2 9351 2854

E-mail address: jun.huang@sydney.edu.au (Jun Huang) and yijiao.jiang@mq.edu.au (Yijiao Jiang)

Abstract

Ketonization can efficiently convert carboxylic acids into ketones, promising in bio-oil upgrading when coupled with fast pyrolysis of biomass. For economic-sustainable bio-refining, Ca/Zn/AlO_x (CZA) metal oxides with various Ca/Zn/Al ratios have been prepared by the low-cost and natural abundant metals in the process. Mechanism study on the ketonization of acetic acid revealed the reaction pathways strongly depends on “composition-structure-function” of Ca/Zn/AlO_x catalysts. The reaction is mainly performed on strong base sites (e.g. CaO and ZnO) via thermal decomposition of acetates at high temperature (≥ 375 ^oC), but depends on acid-base pairs (e.g. amorphous calcium aluminates) significantly at low temperature (≤ 350 ^oC). CZA(331) (Ca/Zn/Al = 3/3/1) obtained the highest acetone yield of 97.1 % at 425 ^oC hitherto and retained for over 100 h with simple regeneration process. Adding major bio-oil model compounds (e.g. phenol) into the reaction mixture has minor effect on CZA(331)catalysts. Therefore, current highly active and stable CZA catalysts are promising in boosting the efficiency and economy of bio-oil upgrading process in future.

1 Introduction

The increasing demand for fossil fuels and environmental issues drives the rapid development of renewable biomass-derived fuels that can directly replace fossil fuels in the current infrastructure in a green and economic way [1]. Fast pyrolysis of lignocellulosic biomass is a major route to yield liquid bio-fuels with high yield (up to 80 %) [2]. Fast pyrolysis oil contained furanics, phenolics, carboxylic acids (e.g. 10 wt% acetic acid in bio-oil produced from sawdust), water (30-40 %) and other oxygenates [3-6]. The obtained bio-oil is instable, corrosive (pH of 2-3), high viscosity and low heating value (16-19 MJ/kg) [1, 7]. It can be upgraded through hydrodeoxygenation or zeolite upgrading [8-11]. The former consumes a large amount of expensive hydrogen [12], while the latter results in poor hydrocarbon yields and high coke formation [13], which limit their industrial applications.

Carboxylic acids is one of the most oxygen-abundant group in bio-oils [14], in the form of acetic acid, butyric acid and formic acid and etc. [15]. The ketonization reaction can efficiently convert carboxylic acids into ketones via C-C coupling, which can significantly increase the energy density and stability of bio-oil along with raising the pH [16]. It is a clean and environmental friendly chemical process and no solvent is necessary [1, 17, 18]. Moreover, ketones are desired building blocks and readily to be converted into long-chain hydrocarbons via aldol condensation followed by hydrogenation [1], increasing the yield of transportation fuels [19]. When coupled with fast pyrolysis, ketonization has attract great attention both economically and technically.

Solid catalysts, including metal oxides and mixed metal oxides, hydrotalcites and zeolites, have been widely studied on ketonization of carboxylic acids [1, 18]. Amphoteric reducible metal oxides (e.g. CeO_2, TiO_2, and ZrO_2) is widely accepted as the most active catalysts for ketonization [1, 20-22]. Their high activity has been attributed to surface acid-base properties, which allows carboxylic acid adsorbed adjacently for ketonization via ketene [20, 23] or β-ketoacid [24, 25] based reaction mechanisms. In ketonization of acetic acid (AcOH), the most abundant carboxylic acid compound in bio-oils [10, 26, 27], supported CeO_2 catalysts exhibit much higher activity (93.1 % acetone yield over CeO_2/1%K_2O/Al_2O_3) and stability (97 %

conversion of AcOH for 96 h over CeO_2/SiO_2) [7] than these over hydrotalcites (86.5-89 % yield of acetone) [28, 29] and zeolites (100 % acetone selectivity with very low AcOH conversion) [30, 31]. However, these amphoteric reducible metal oxides are expensive and low abundant in nature. Thus, it is desired to developing novel metal oxide catalysts with low cost but highly active and stable for ketonization reaction.

Solid bases, including CaO, MgO and ZnO [32], are active catalysts for ketonization of carboxylic acids [7, 21, 33]. These strong bases with low lattice energy can transfer carboxylic acids into metal acetates, followed by thermal decomposition to produce acetone [34]. These bases supported on SiO_2 provide a yield of acetone from acetic acid in a range of 33-59 %, much lower than 97 % over CeO_2/SiO_2 [21]. Alumina is a widely utilized support material to promote the dispersion of metal particles. It can form metal aluminates in mixed metal oxides, e.g. calcium aluminates [35] and zinc aluminates [36, 37]. These mixed metal oxides (CaO/Al_2O_3 and ZnO/Al_2O_3) are thermally stable after calcination at 800 ^oC [35, 38]. Moreover, alumina with strong Lewis acidity can promote the adsorption of carboxylic acid on catalyst surface. In well mixed metal oxides, it is probably to enhance the concentration of carboxylic acids in the local structure of basic sites (e.g. CaO) to improve their catalytic activity, and thus, promising for ketonization.

In this work, $Ca/Zn/AlO_x$ (CZA) composited metal oxides were synthesized for ketonization of acetic acid. XRD pattern and microscopy were utilized to investigate the morphology of CZA catalysts and confirm the presence of CaO, ZnO, $ZnAl_2O_4$ and amorphous alumina and calcium aluminates. The surface basicity of these catalysts has been studied by TPD-CO_2. Combined with the reaction results of ketonization of acetic acid, two reaction mechanisms based on temperature dependence has been proposed. These CZA catalysts exhibit high activity and stability comparable to CeO_2/SiO_2 that has been reported as the best catalyst for this reaction [7, 21], and are easily to be regenerated. Finally, the stability of CZA catalysts was further investigated by furfural and phenol addition to reaction mixture individually, which are the major compounds in pyrolysis bio-oil [2, 26, 39].

2 Experimental

2.1 Catalyst preparation

$Ca/Zn/AlO_x$ catalysts with various atomic ratios were synthesized by co-precipitation method. $Zn(NO_3)_2{\cdot}6H_2O$, $Ca(NO_3)_2{\cdot}6H_2O$, $Al(NO_3)_3\ {\cdot}9H_2O$ were purchased from Sigma-Aldrich and used as precursors. Precursors with desired amount of Ca/Zn/Al molar ratios of 1:1:1, 2:2:1, 1:1:3, 3:3:1, 1:1:2, 2:1:2, 3:2:3 and

1:2:1, were prepared by dissolving certain amount of metal salts in deionized water. The precursor mixture was precipitated with saturated Na_2CO_3 solution drop by drop under stirring, with keeping the pH of the suspension within 7-9 at 60 °C. After co-precipitation, the resulting suspension was aged under agitation for an hour and then filtered under vacuum. The filter cake was rinsed with deionized water, and then dried at 80 °C overnight. Finally, the solid products were calcined at 800 °C for 4 h in static air with a heating rate of 1 °C/ min. The nomenclature of obtained $Ca/Zn/AlO_x$ catalysts is defined as CZA(XYZ), where X, Y and Z are the mole ratios of Ca, Zn and Al, respectively.

2.2 Catalyst characterization

X-ray diffraction (XRD) patterns of $Ca/Zn/AlO_x$ catalysts were collected in the range of 10-70° with a SIEMENS D6000 e diffractometer quipped with Cu-Kα radiation (λ = 0.154 nm, 35 kV, 40 mA).

The specific surface areas of $Ca/Zn/AlO_x$ samples were determined by N_2 adsorption/desorption isotherms on an Autosorb IQ-C system. An amount of 150 mg of each sample was degassed at 150 °C for 12 h under vacuum before the measurements and then recorded at 77 K.

The scanning electron microscopy (SEM) coupled with Energy-dispersive X-

ray spectroscopy (EDXs) was used to investigate the surface morphology and the element distributions of CZA catalysts. Before scanning, samples were coated with gold under vacuum. Coating intensity and time was 25 mA and 150 s, respectively. Then the images were recorded on a FESEM, Zeiss Ultra+.

The phases and microstructure of $Ca/Zn/AlO_x$ samples were obtained by using a transmission electron microscopy (TEM) JEOL 2200FS with sample, which were mounted on a carbon coated copper grid by drying a droplet of a suspension of the ground sample in ethanol.

Temperature programmed desorption using CO_2 as probe molecule (TPD-CO_2) was used to determine the basicity of CZA catalysts under study. Prior to TPD, sample (50 mg) was loaded and degassed at 450 ^oC for 1 h under N_2 flow to completely remove molecules adsorbed on catalyst surface. The sample was saturated with CO_2 at 50 ^oC for 15 min, flushed with N_2 for 15 min, and then desorbed with CO_2 (total flow of 80 ml/min) from 50 to 650 ^oC with a ramp of 10 ^oC/min. The desorption gas were analyzed by a Mass Spectrometer connected to TPD system.

2.3 Ketonization of acetic acid

The catalytic performance of CZA catalysts were tested in a continuous reaction

system. The catalyst (100 mg) was pretreated under nitrogen flow of 30 ml/min for 30 min at 400 °C. Reactant of 50 wt% aqueous AcOH solution was pumped into the reactor at a flow rate of 0.4 mL/h with N_2 as carrier gas (10 ml/min). The reaction products were condensed in an ice-water trap and collected hourly for GC analysis. The conversion of AcOH and composition of the product mixtures were qualified using a Shimadzu GCMS-QP2010 Ultra with a RTX-5MS capillary column (30 m × 0.25 mm × 0.25 μm) and quantified by Shimadzu GC–FID equipped with a RTX-5 capillary column (30 m × 0.32 mm × 3 μm).

The stability and tolerance of CZA catalysts were tested by adding furfural or phenol, both are major compounds in pyrolysis bio-oil. Furfural or phenol (10 wt%) was mixed with acetic acid (40 wt%) and water (50 wt%) as the reaction feed. All other reaction conditions are the same as described above. The used CZA catalyst was calcined in situ at 425 °C for 1 h for recycle by using air to replace reaction mixture and N_2.

3 Results and Discussions

3.1 Catalyst characterizations

The XRD patterns of Ca/Zn/AlO_x mixed oxides catalysts with various Ca/Zn/Al atomic ratios are displayed in Fig. 1. It shows the Ca/Zn/AlO_x consists of four

compounds as ZnO, $ZnAl_2O_4$, CaO and $Ca(OH)_2$. No crystalline Al_2O_3 can be observed in all samples. CZA(121) (Fig. 1h) possessing the largest amount of Zn content exhibits the diffraction peaks at 31.5°, 34.2°, 36.0°, 47.2°, 56.3°, 62.5°, 66.2°, 67.8°, and 69.0°, corresponding to the ZnO crystal faces of 100, 002, 101, 102, 110, 103, 200, 112 and 201, respectively [40, 41]. Reducing the atomic fraction of Zn can lower the intensity of these diffraction peaks. With the Zn fraction lower than 1/3 (Fig. 1a-d), the diffraction peaks of ZnO become broad and their intensity significantly decreased. Instead, the diffraction peaks at 31.0°, 37.0°, 44.5°, 56.5° and 59.0°, corresponding to $ZnAl_2O_4$ having the crystal faces of 220, 311, 400, 422 and 333/511 [42], were strongly enhanced (Fig. 1a-d). Increasing the intensity of $ZnAl_2O_4$ correlates well with reducing the Zn/Al ratio (CZA(113) > CZA(212) > CZA(112) > CZA(323) > CZA(111)). This is caused a higher concentration of Al can promote the solid reaction between ZnO and alumina to generate $ZnAl_2O_4$ particles under high calcination temperature (e.g. 800 °C) [38]. The diffraction peaks of CaO at 32.0°, 37.1°, 53.6°, 63.8° and 67.1°, corresponding to the crystal faces of 111, 200, 220, 331 and 222 [43, 44], were detected with CZA(331) (Fig. 1g) having the largest Ca fraction. When exposed in the air, partial of CaO can be rehydrated to $Ca(OH)_2$, showing diffraction peaks at 17.7° and 28.0°. No crystalline phase between Ca and Zn species can be detected, similar as that

reported previously that only pure CaO and ZnO can be observed in CaZnO mixed metal oxides [40].

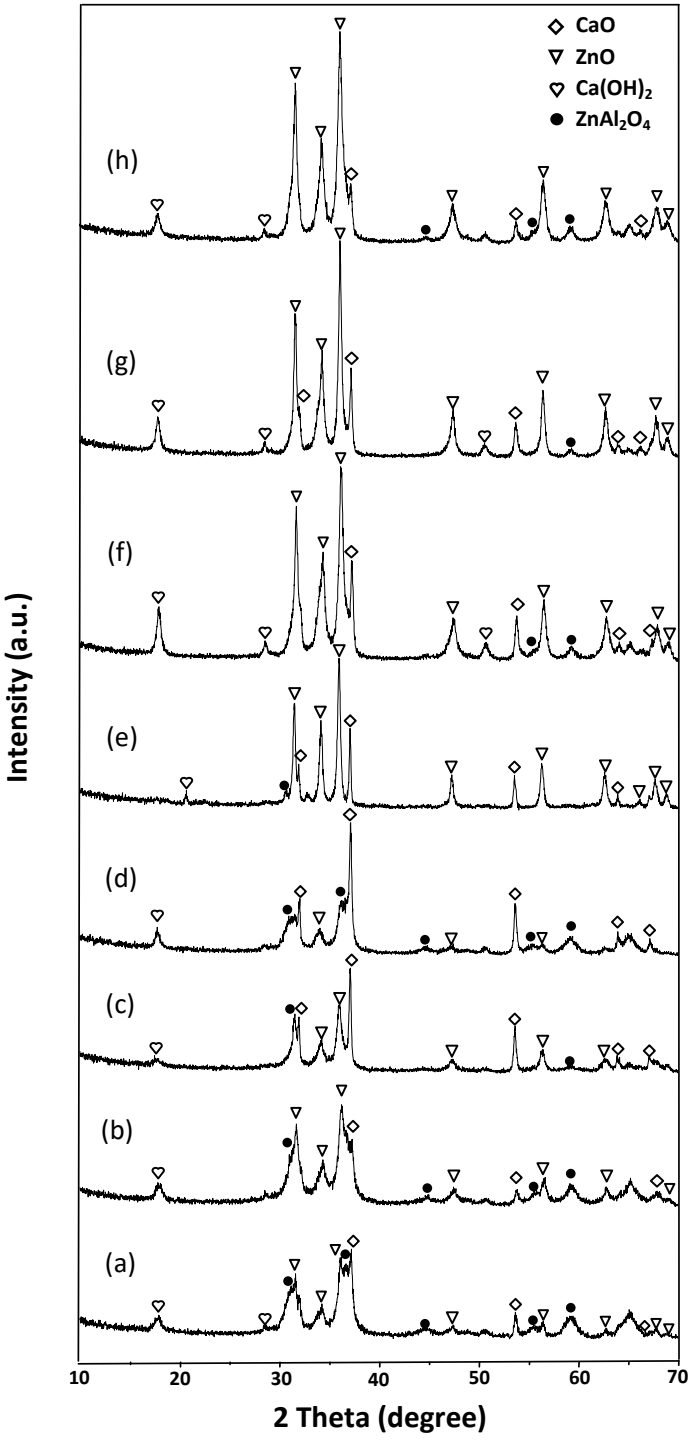

Figure 1. XRD patterns of Ca/Zn/AlOx catalysts. (a) CZA(113), (b) CZA(112), (c) CZA(323), (d) CZA(212), (e) CZA(111), (f) CZA(221), (g) CZA(331) and (h)

CZA(121).

The particle size and specific surface area of the catalysts are summarized in Table 1. The specific surface area of the $Ca/Zn/AlO_x$ is in the range of 11.6-62.2 m^2/g. With Ca content $\geqslant$ 33.3 % (CZA(111)), a relative low specific surface area ($\leqslant$ 36.7 m^2/g) was obtained. When lower the Ca content $\leqslant$ 25 % and increased the Al content $\geqslant$ 25 %, the specific surface area significantly enhanced for over 58 %, up to 58.0-62.2 m^2/g. This has been explained by the strongly increase of CaO particle size at high Ca content. Clearly, alumina as support materials can significantly improve the dispersion of Ca and Zn species with increasing the Al content, resulting in smaller particles size on surface, e.g. CZA(113) having largest Al content obtained smallest particle size of CaO, ZnO and $ZnAl_2O_4$ among all samples. CZA(121) obtained the largest surface area, which is probably due to the formation of different morphology and structure.

Table 1. Specific surface area and crystal size of $Ca/Zn/AlO_x$ catalysts

Catalyst	Specific surface area (m^2/g)	Particle size (Å)[a]		
		CaO	ZnO	$ZnAl_2O_4$
CZA(111)	11.6	482	265	276
CZA(323)	19.1	317	167	243
CZA(331)	21.4	284	228	236
CZA(221)	23.9	263	172	177

CZA(212)	36.6	291	126	133
CZA(112)	58.0	207	110	162
CZA(113)	61.4	123	85	76
CZA(121)[b]	62.2	-	-	-

[a] Calculated from FWHM (full width at half maximum) of the most intense peaks by Scherrer Equation: $D_c = K\lambda /(\beta \cos \theta)$, where K is the shape factor, λ is the wavelength of x-ray, β is the line broadening in radians at FWHM, and θ is the Bragg angle and D_c is the mean particle size [45]. [b] The determination of each particle size is difficult due to the strong overlap of these peaks.

The morphology of these mixed metal oxides was investigated by scanning electron microscope (SEM) as shown in Fig. 2. CZA(111) (Fig. 2a) exhibits the largest particle size and strongly agglomerated, possibly resulted in the largest particles size and lowest specific surface area among CZA samples (Table 1). For CZA(221) (Fig. 2b) and CZA (331) (Fig. 2d) with high concentration of Ca and Zn, the spherical metal particle (CaO and ZnO) are well-dispersed and stabilized on AlO_x surface [46] in the range of 15–30 nm, which is consistent with those reported in Table 1. The images of CZA(113), (112), (212) and (323) (Image c, e, f and g) show a crosslinked surface, which is attributed to alumina, amorphous alumina or aluminate compounds [47-49] formed at high Al concentration (≥ 37.5 mol%). The large CaO particles (20 nm) and small round-shaped ZnO particles (10 nm) has been identified [50, 51], well in line with those reported in Table 1. The $ZnAl_2O_4$ particles, formed by ZnO and alumina at high temperature (e.g. 800 ^oC) [38], are

agglomerated inside the crosslinked structure of alumina [52] and hardly to be identified on surface. In Fig. 2h, CZA(121) with the highest Zn content (50 mol%), exhibits a flake-like morphology, similar to layered double hydroxides (LDHs) catalysts [53]. LDHs are often featured with large surface areas [54], and possibly, affords a specific surface area of 62.15 m^2/g for CZA (121), which is the largest among all the CZA catalysts.

The elemental analysis of CZA samples were studied by SEM coupled with EDX, and the EDX mapping images of CZA(113) and CZA(331) were shown in Fig. 3. CZA(113) with highest Al content exhibits a very bright color in Fig. 2a, corresponding to an alumina-rich phase. A well dispersion of Ca and Zn species on alumina surface were observed, but their relatively low content lead to dark and blurry images (Figs. 3b and c). The clear images of Ca and Zn species (Figs. 3e and f) were observed with CZA(331) having higher Ca and Zn content, while the Al mapping image is blurred (Fig. 3d) due to its low content. No single crystalline alumina-rich phase can be detected, confirmed the observation in XRD patterns. In both samples, the Al and Zn mapping images are very similar, which indicates a co-existence on their distribution. This may be caused by the formation of a solid solution between ZnO and alumina, resulting in $ZnAl_2O_4$ under high temperature

calcination [38] (e.g. 800 °C), well in line with the observation in XRD and SEM images.

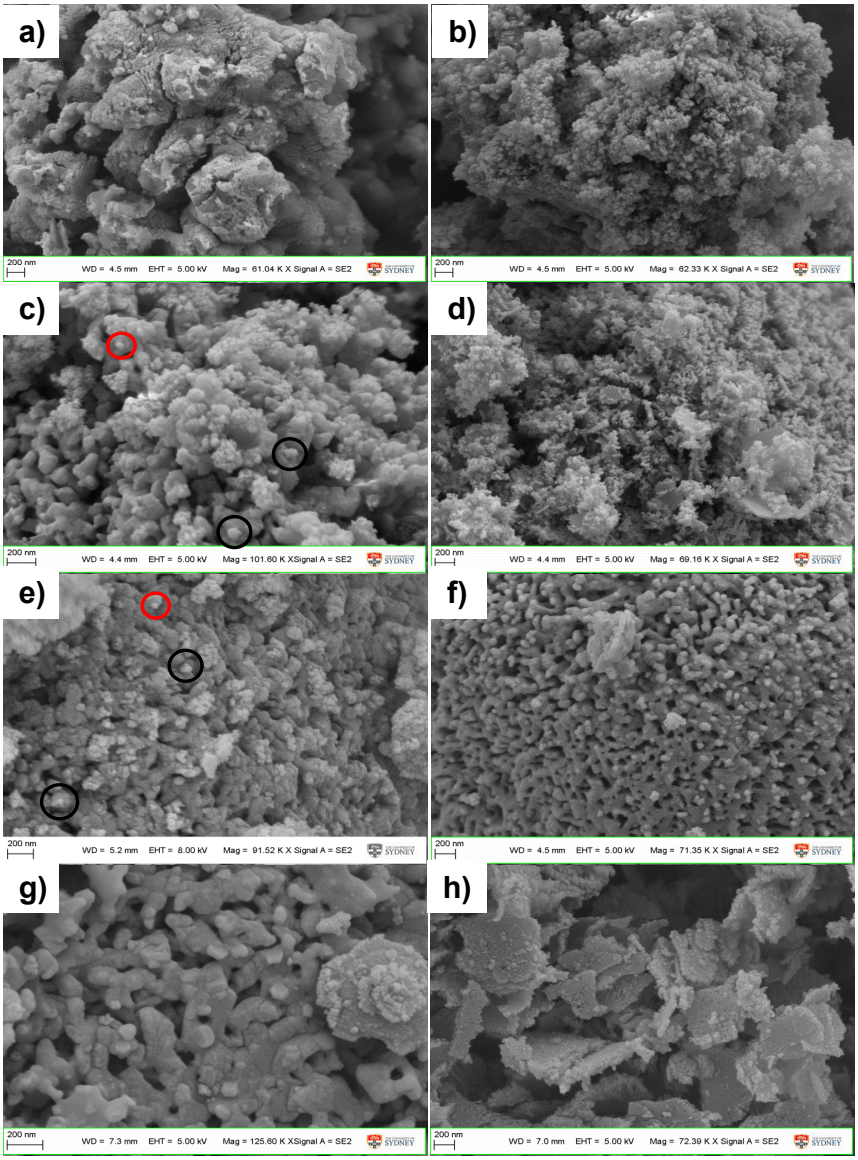

Figure 2. SEM results of Ca/Zn/AlO_x catalysts. (a) CZA(111), (b) CZA(221), (c) CZA(113), (d) CZA(331), (e) CZA(112), (f) CZA(212), (g) CZA(323) and (h) CZA(121). The CaO and ZnO particles identified are marked in black and red

circles in images c and e, respectively.

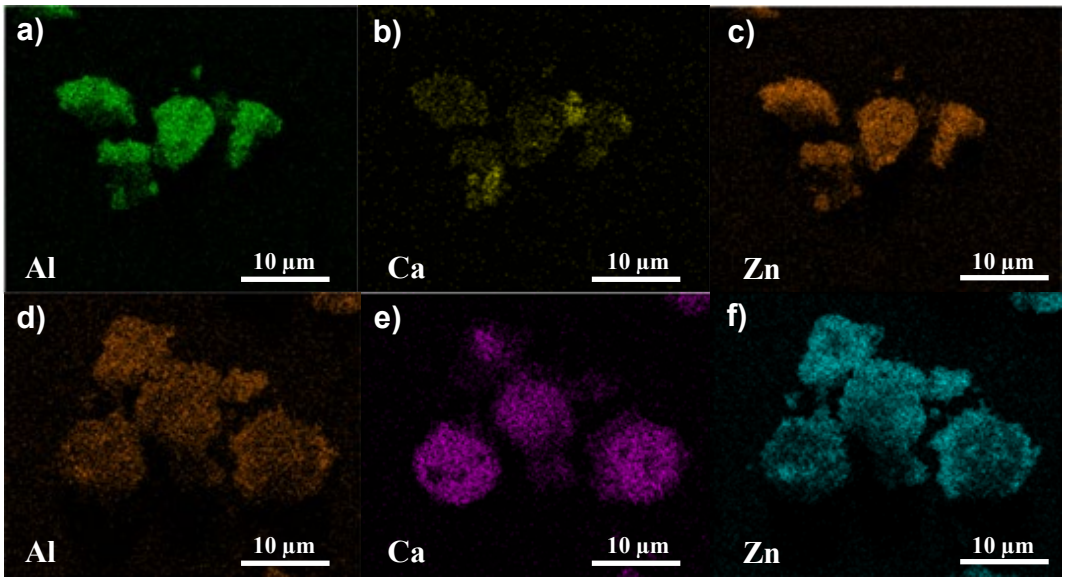

Figure 3. EDX image of CZA(113) (a-c) and CZA(331) (d-f).

HRTEM images of CZA catalysts are shown in Fig. 4. Two different types of crystals were observed in Fig. 4a, which are assigned to ZnO (18 nm) and CaO (40 nm), respectively, correlated well with XRD analysis. Similarly in Fig. 4b and c, small crystals with size of 10~15 nm are assigned to ZnO, which is the major component in CZA(113) and CZA(331) by XRD analysis. CZA(331) shows an amorphous structure that similar to amorphous Al_2O_3 as reported previously [55], which is different from CZA(111) and CZA(113) with higher Al content. The latter two exhibit an amorphous structure of calcium aluminates, which is stable under calcination at 800 ^oC and directly converted into corresponding crystal at T > 883 ^oC [35]. As

shown in Fig. 3b and c, the image of Ca is obviously blur than that of Zn, which may confirm Ca incorporated into the Al matrix and hardly to be detected compared to Zn. Besides ZnO and CaO, a cross-direction structure with an angel of ca. 40^{o} was observed with CZA (121) (Fig. 4d), assigned to $ZnAl_2O_4$ [56], the size of which is 15 nm and correlates well with XRD analysis.

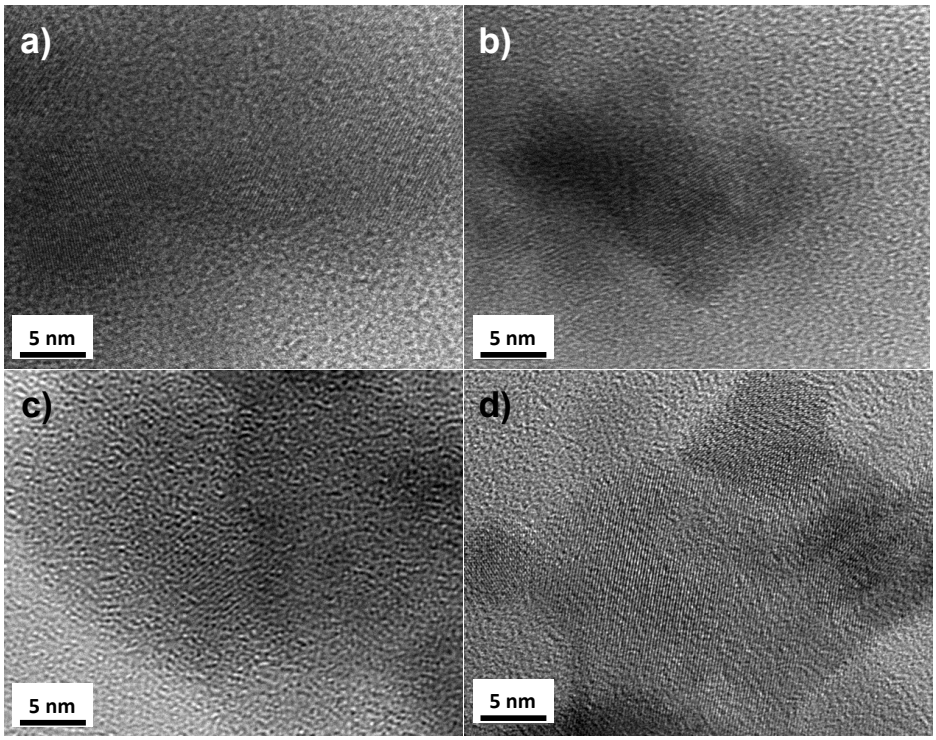

Figure 4. TEM of Ca/Zn/AlO_x catalysts. (a) CZA(111), (b) CZA(113), (c) CZA(331), (d) CZA(121).

Based on XRD and microscopy analysis, the distribution of basic metal oxides (CaO and ZnO) on alumina and their mixed oxides with alumina has been well studied. These metal oxides are well distributed on alumina surface in amorphous

domain at Al content ≥ 37.5 %, but form large crystals at higher Ca and/or Zn content. These basic metal centers are potential active sites for base-catalyzed ketonization of acetic acid. Therefore, the distribution and density of these surface basic site were evaluated using TPD-CO_2 (Fig. 5). Both CZA(331) and CZA(121) with higher metal content exhibit CO_2-desorption peaks in the temperature ranges of T < 200 °C, 200 °C < T < 400 °C, and T > 400 °C, corresponding the existence of weak, medium and strong basic sites in these samples [40, 57]. CaO and ZnO are metal oxides possessing mainly strong to very strong basicity [32], corresponding to the peak at T > 400 °C [40, 57] associated with isolated O^{2-} on surface [58]. The medium to weak basic sites are due to alumina and metal aluminates [58, 59], e.g. only peaks at temperature T < 400 °C can be observed with TPD-CO_2 of $ZnAl_2O_4$ and attributed to surface M^{n+}–O^{2-} pair [58], while surface hydroxyl groups may adsorb CO_2 at low temperature and act as weak basic sites as well [59, 60]. The higher peak intensity demonstrates CZA(331) has more basic sites than CZA(121) at each temperature range. With increasing the Al content, the CZA(111) provides the highest density of basic sites but mainly in medium strength (Fig. 5c). Further increasing the Al content with lowest (Ca+Zn) content in CZA(113) (Fig. 5d), leads to the lowest density of surface basic sites with medium strength among all the CZA catalysts. It is probably caused by a large extent of Ca

and Zn mixed with alumina to form metal aluminates, e.g. metal components are well dispersed on CZA(113) surface (Fig. 1a), providing mainly moderate basicity.

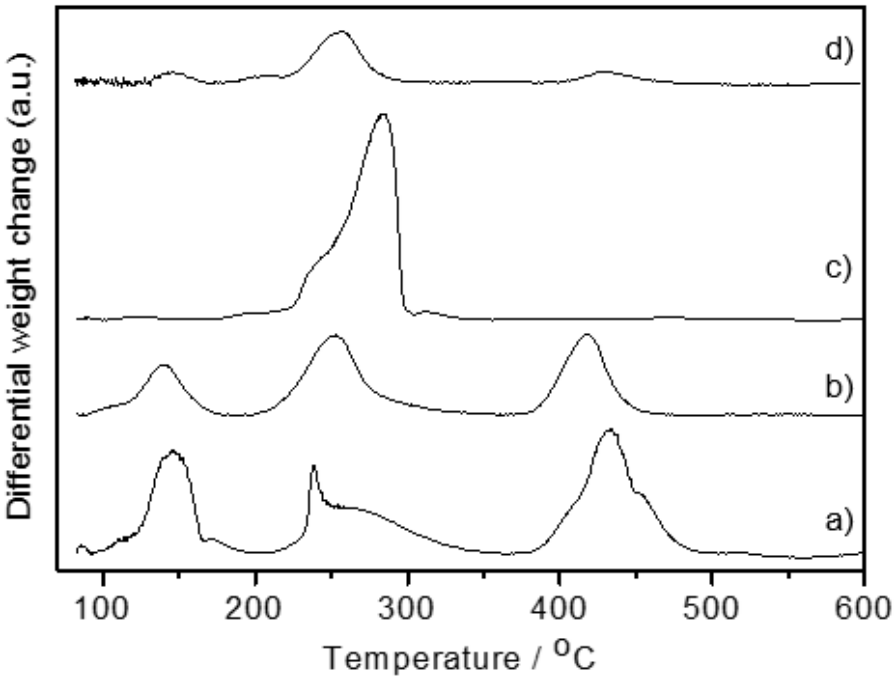

Figure 5. CO_2-TPD of Ca/Zn/AlO_x catalysts. (a) CZA(331), (b) CZA(121), (c) CZA(111), (d) CZA(113).

3.2 Ketonization of acetic acid on Ca/Zn/AlOx

Strong basic metal, e.g. CaO, are active catalysts for base-catalyzed ketonization of acetic acid [61]. Based on TPD-CO_2, current Ca/Zn/AlO_x catalysts exhibit weak to strong basicity are promising for ketonization of acetic acid. Moreover, the crosslinked structure and well-dispersed metal oxides were observed by SEM and EDX, with amorphous to crystalline morphology. It might enhance the catalytic

activity and stability of Ca/Zn/AlOx, and thus, tested in ketonization of acetic acid under various temperature and water loading, with furfural or phenol as additives.

3.2.1 Effect of reaction temperature and CZA compositions

Ketonization of AcOH is often carried out under temperature between 300 °C and 450 °C [29]. At this range, both catalytic conversion and thermal pyrolysis of acetic acid are possible to take place [17]. The pyrolysis of acetic acid can be performed in two different ways [62]: AcOH can be decomposed into 1) ethenone at a temperature of 400 °C; or 2) to carbon dioxide and methane at reaction temperature from 460 to 600°C. By using sand as a reference catalyst, the pyrolysis of AcOH (2~3%) is negligible at $T \leq 375$ °C. Under 400 °C < T < 425 °C, the AcOH conversion enhanced to 10 and 17%, respectively, while no CO_2 and CH_4 was detected. Thus, ketonization of AcOH was performed between 300 and 425°C.

The catalytic conversion of AcOH and selectivity to acetone on Ca/Zn/AlO_x with various Ca/Zn/Al molar ratios and temperature range was summarized in Table 2. The conversion of AcOH over CZA catalysts are quite low (≤ 44 %) at $T \leq 325$ °C, which dramatically raised to 70 % with increasing the reaction temperature to 375 °C, and further enhanced to 93-100 % at 425 °C. In the meantime, the selectivity

to acetone remains 100 % at $T \leq 375$ °C for all CZA catalysts, but slightly decreased to 97.1-99.5 % over CZA(331), CZA(221) and CZA(111) at temperature of 400-425 °C. CZA(121) with highest Zn content, it shows a highly crystalline LDHs-like structure that is mainly in ZnO domain. ZnO is known as a weaker base than CaO [51], while $ZnAl_2O_4$ possesses only weak acidity and negligible basicity [37, 63], and thus, not as active as CZA catalysts having higher Ca content for ketonization of AcOH.

Table 1. The conversion of acetic acid and selectivity to acetone on $Ca/Zn/AlO_x$ catalysts.

Catalyst	Conversion of acetic acid (%)						Selectivity to acetone (%)		
	300 °C	325 °C	350 °C	375 °C	400 °C	425 °C	300-375 °C	400 °C	425 °C
CZA(331)	14	44	92	93	99.5	100	100	99.0	97.1
CZA(221)	7	25	47	85	99.6	99.4	100	99.5	98.5
CZA(111)	10	29	38	84	98.9	99.0	100	100	98.9
CZA(112)	8	31	42	82	97.3	98.9	100	100	100
CZA(212)	20	27	51	81	96.1	96.3	100	100	100
CZA(113)	13	31	39	71	90.4	94.0	100	100	100
CZA(323)	16	34	55	74	87.7	93.0	100	100	100
CZA(121)	19	25	52	70	87.1	94.5	100	100	100

CZA(331) exhibit the highest catalytic activity among all the catalysts in all temperature range except 300 °C. An AcOH conversion of 92 % was obtained

compared to other's under 55 % at 350 °C. As revealed by TPD-CO_2, this correlates well with the strongest basicity obtained with CZA(331) due to its highest Ca and Zn content. Similarly, CZA(221) and CZA(111) both exhibit higher activity than the other having lower Ca and Zn content at $T \geq 375$ °C. Since no by-products anhydride or ethenone can be detected, the catalytic decompose of AcOH to CO_2 and methane [64] (see Eq. 4, which carried out at 460 °C without catalysts based on an ab initio study [65]) corresponds to lowering the selectivity to acetone can be expected at high temperature (e.g. ≥ 400 °C).

One should be noted, that CZA(323) with similar (Ca+Zn) content leads to a much lower acetone yield (74 %) than that obtained with CZA(111) (84 %) at $T \geq$ 375 °C. A clearly difference is CZA(323) in a large extent of amorphous domain, compared to highly crystalline CZA(111) (see Fig. 1). As discussed in the microscopy investigations (Fig. 3 and 4), calcium aluminates were formed in the amorphous phase,, which mainly provides moderate basicity as observed in the TPD-CO_2 experiments. The formation of $ZnAl_2O_4$ possesses only weak acidity and negligible basicity [37, 63]. The lack of basicity in CZA(323), thus afforded the lower activity than those obtained with CZA(111) $T \geq 375$ °C. However, CZA(323) exhibits higher activity than CZA(111) at $T \leq 350$ °C, compared to CZA(221) and CZA(111). It was further confirmed by CZA(212), CZA(112) and CZA(113) with lower (Ca+Zn)

content but increasing amorphous domain, resulting in a higher activity than higher crystalline CZA(221) and (111) at low temperature (≤ 350 °C). It clearly demonstrates the yield of acetone from ketonization of AcOH strongly depends on the catalyst basicity and reaction temperature, probably via two different reaction pathways over CZA catalysts.

3.2.2 Reaction Mechanism

On alkali and alkali earth oxides, a widely accepted ketonization mechanism is AcOH can be strongly adsorbed on low lattice energy bases to form bulk acetates, followed by thermal treatment to release acetone and CO_2 in the gas phase [34]. The thermal decomposition of acetates can be significantly enhanced with increasing reaction temperature, but hampered at low temperature [66]. Here, both CaO and ZnO, as well as $ZnAl_2O_4$ are oxides with low lattice energies [36], while the latter is inactive in ketonization [37, 63]. CZA catalysts (CZA(331), CZA(221) and CZA(111)) with highly crystalline structure and high content of Ca and/or Zn exhibit much higher basicity than CZA in amorphous domain (e.g. CZA(113)) as revealed by TPD-CO_2 analysis (Fig. 5). Our reaction results shows the activity of CZA catalyst correlates well with their basicity and are highly active at high temperature (T ≥ 375 °C). An AcOH conversion of 70-100 % was obtained, which strongly reduced to 7-55 % at T ≤ 350 °C (Table 2). It demonstrates the thermal

decomposition of acetates is one of the major routes for ketonization of AcOH over CZA catalysts, particularly work at high temperature as shown in Scheme 1.

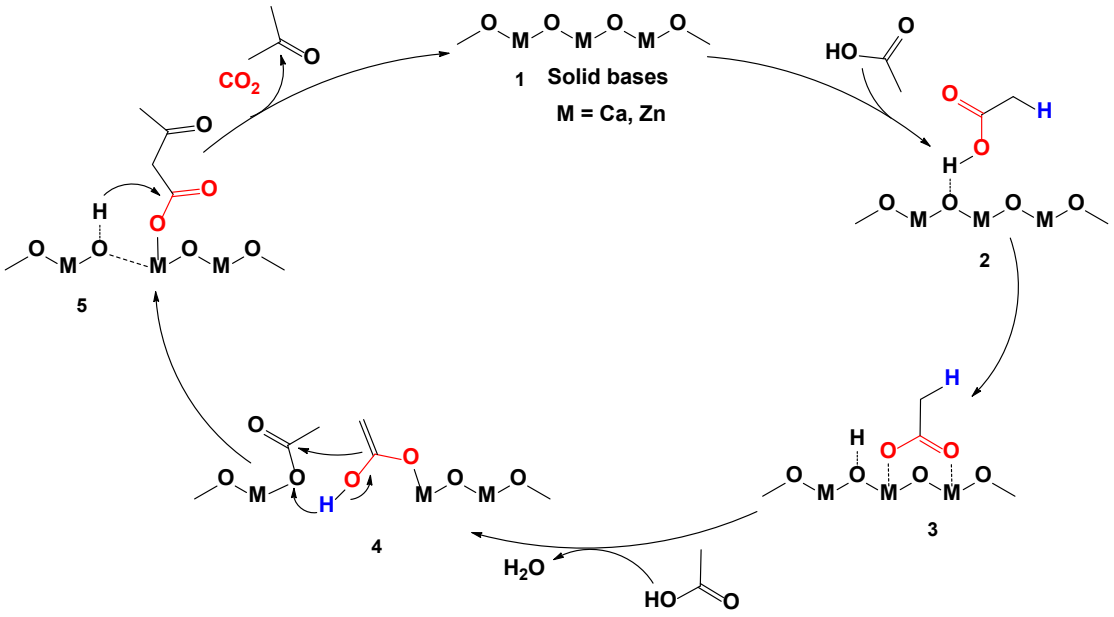

Scheme 1. Proposed mechanism of catalytic ketonization over CZA catalysts at high temperature.

At low temperature, the catalytic performance of CZA catalysts with less Ca but higher Al content provides higher AcOH conversion than that obtained with CZA in highly CaO and ZnO domain (Table 2). Clearly, an alternative reaction pathway dominates ketonization at low temperature. The temperature-controlled reaction pathway has been previously reported for Fe_2O_3 [25] and CeO_2 [67]. For ketonization over Fe_2O_3 [25], the reaction is carried out via thermal decomposition of bulk acetate at high temperature (> 400 ^oC), while at low temperature, it

proceeds via a catalytic reaction pathway requiring acid-base pair sites.

Ketonization of carboxylic acid in gas-phase based on acid-base pair sites has been proposed for oxides with high lattice energies [1, 17, 23, 64, 68]. It requires basic sites for dissociative adsorption of carboxylic on surface, which can react with another carboxylic acid stabilized and activated on neighboring Lewis acid sites. Amphoteric reducible metal oxides (e.g. CeO_2, TiO_2, and ZrO_2), providing both medium strength Lewis acidity and basicity [32], are better catalysts than pure acidic or basic oxides for ketonization [1], since it can balance the acid-base properties for carboxylic acid adsorption and activation on surface.

Both pure CaO and ZnO have strong to very strong Lewis basicity with very weak acidity [32], which only provide very few acid-base pairs on surface [44]. The surface basic sites, e.g. coordinatively unsaturated oxygen ($Ca\text{-}O^{2-}$) and hydroxide ($Ca–OH^-$) sites [44], is able to strongly adsorb AcOH to form bulk acetates at low temperature, which can be decomposed at high temperature [34]. On the other hand, Al_2O_3 with strong Lewis acid sites [32] can strongly adsorbed AcOH [34, 69]. However, it consists of nearly no acid-base pair sites as revealed by FTIR investigation [69], which is nearly inactive for catalytic ketonization conversion.

The catalytic performance of CZA catalysts increased in line with increasing calcium aluminates formed in amorphous domain at low temperature, which has

been observed in Table 2 combined with XRD pattern. The EDX mapping images (Fig. 3b and c) shows Ca can be incorporated into the Al matrix, resulting in well-mixed CaO and Al_2O_3 oxides in amorphous calcium aluminates, which is different from the formation of binary metal oxides, such as crystalline $ZnAl_2O_4$. It is possible to provide strong basic sites on CaO in spatial proximity to the Lewis acid sties on Al_2O_3 as shown in Scheme 2 middle. Carboxylates can be formed on CaO through AcOH dissociated on surface basic oxygen sites upon adsorption, and carboxylates (CH_3COO^-) bind to two surface cations in a bidentate bridging configuration **2** [70], which are energetically more favourable [71]. **2** can be enolized to form **3**, which is more energetically favourable than direct α-hydrogen (hydrogen in blue) abstraction [22, 24]. The enol **3** then undergoes nucleophilic attack by another AcOH adsorbed on neighboring Lewis acid sites from Al_2O_3. The resulting β-ketoacid **4** can be further decomposed into acetone and CO_2, and release the acid-base pair sites to the reaction cycle.

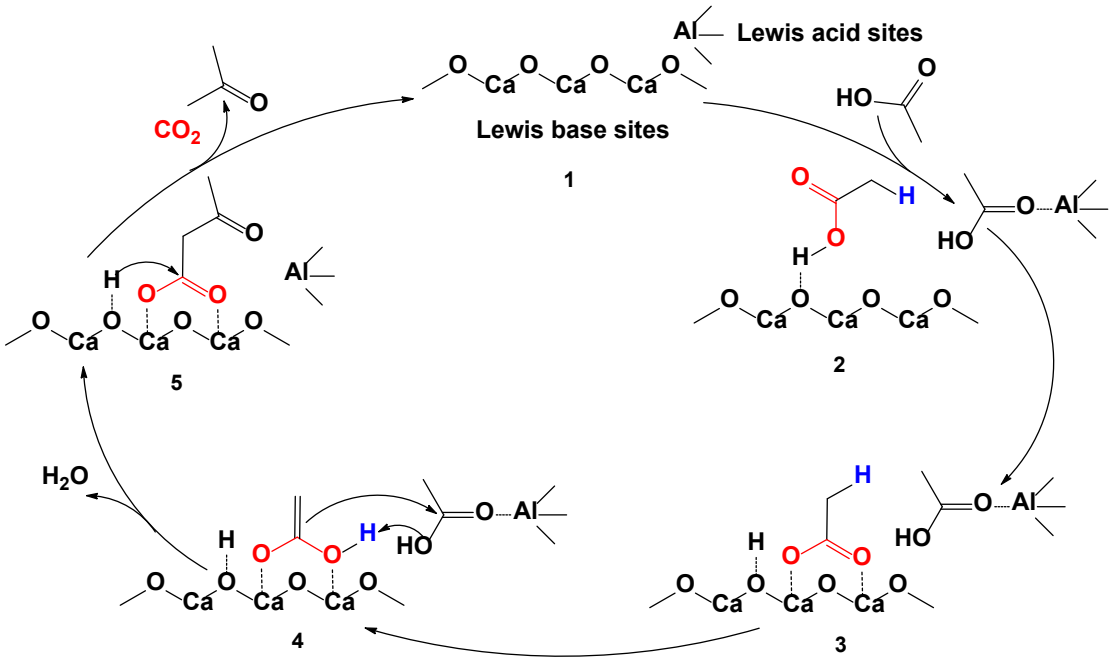

Scheme 2. Proposed mechanism of catalytic ketonization over CZA catalysts at low temperature.

3.2.3 Effect of furans and phenol on the ketonization of acetic acid

Furans and derivatives, derived from hemicellulosic and cellulosic materials by fast pyrolysis, is one of the major of compounds in the bio-oil [2], while phenol is a primary compound in pyrolysis oil from lignocellulosic materials [72]. Therefore, 10 wt% furfural or phenol was added to the aqueous AcOH to evaluate the effect of furans on the ketonization of AcOH. CZA(331) and CZA(221) with the highest activity were selected for further study as shown in Fig. 6.

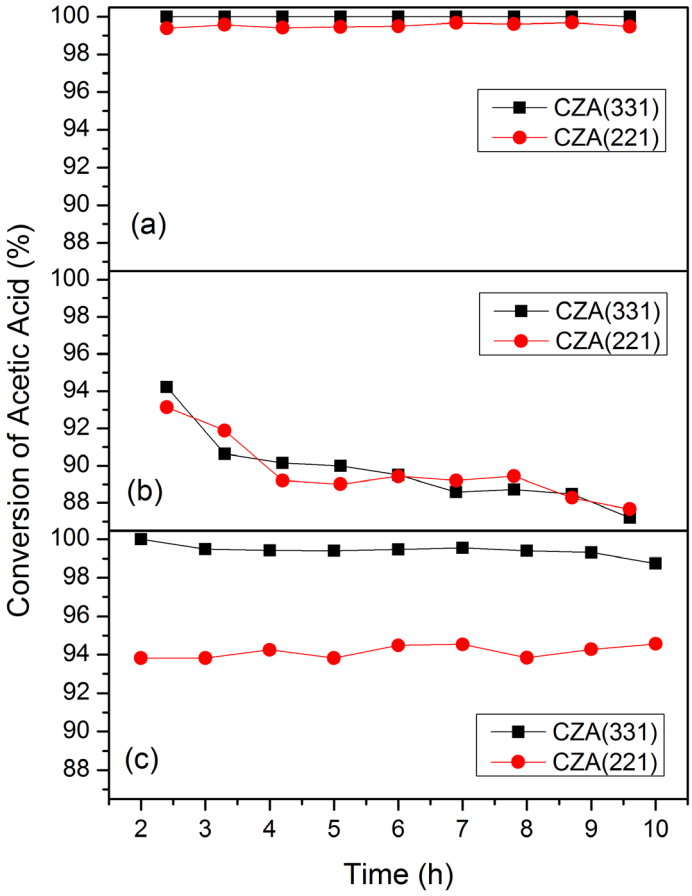

Figure 6. Conversion of acetic acid on CZA(331) and CZA(221) at 425 °C: (a) 50 wt% aqueous acetic acid, (b) 10 wt% furfural added to (a), (c) with 10 wt% phenol added to (a). Reaction was carried out under 425 °C for 10 h.

The conversion of 50 wt% aqueous AcOH kept constantly at 100% and 99.4-99.7% over CZA(331) and CZA(221), respectively (Fig 6(a)). Upon furfural addition (Fig 6 (b)), the conversion of AcOH decreased from 94 to 88% and slightly affected on acetone selectivity (from 97.1-98.5 % to 95-96 %) after 10 h reaction over both

catalysts. A similar phenomenon was observed for ketonization of AcOH over CeO_2/1%K_2O/Al_2O_3, where AcOH conversion decreased from 99 to 64 % and selectivity to acetone decreased from 86.7 to 84.9 % after 12 h reaction [7]. This has been attributed to humin-like by-product formed by furfural addition, which could deposit on the catalysts and block the active site [7].

To clarify the effect of furfural on ketonization of AcOH over CZA(221) and CZA(331), the conversion of furfural has been investigated. As shown in Table 3, the conversion of furfural was 38-43 % after 2 h reaction and declined to 18-24 % after 10h reaction over CZA(331) and CZA(221) catalysts, while the selectivity to resulting by-products remained nearly no change. In the meanwhile, the selectivity to acetone was decreased from 97.1-98.5 % in aqueous AcOH to 91-92 % by furfural addition after 2 h reaction, and then increased to 95-96% after 10 h reaction. It clearly demonstrates the primary-generated acetone participated into the side reaction (e.g. trans-furfurylideneacetone in Scheme 3) with furfural and formed secondary product [73]. These by-products can rapidly poison surface active sites for the first 2 h reaction, and gradually for others with time.

Unlikely, with 10 wt% phenol addition (Figure 6 (c)), the conversion of AcOH (99 %) remained no change after 10 h reaction over CZA(331), while that over

CZA(221) decreased from 99 to 94 %. This indicates phenol addition has minor impact on the catalytic activity of CZA catalysts than the addition of furfural. Over both CZA(331) and CZA(221), no by-products associated to phenol conversion can be detected with an acetone selectivity of 100 %. It demonstrate current CZA catalysts are quite stable upon phenol addition.

Table 3. Conversion of furfural and selectivity on Ca/Zn/AlO_x catalysts

Catalysts	Temperature °C	Conversion of furfural (%)		Selectivity (%)					
		2h	10h	TFFA[a]		FA[b]		1-P[c]	
				2h	10h	2h	10h	2h	10h
CZA(331)	425	43	18	75	78	11	9	14	13
CZA(221)	425	38	24	78	80	10	7	12	13

[a] Trans-furfurylideneacetone; [b] Furfural alcohol; [c] 1-pentanol

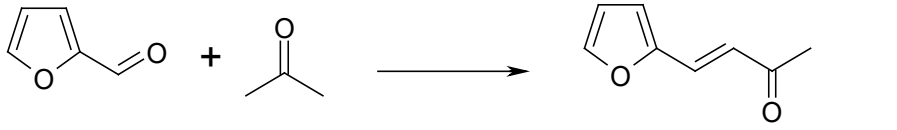

furfural acetone trans-furfurylideneacetone

Scheme 3. Proposed pathway for trans-furfurylideneacetone.

3.2.4 Stability and reusability of CZA catalysts

The stability of CZA(331), the best performance one in this work, was tested for a long-term run under 425 °C with aqueous AcOH. The conversion of AcOH as a function of reaction time has been shown in Fig. 7 (a). The AcOH conversion is

100% at 56 h, slightly decreased to 92% at 72 h, and strongly dropped to 80% at 96 h by following the linear decreasing tendency. The catalyst deactivation may be caused by carbon deposition on active sites [7]. In another run (Fig 7 (b)), the used CZA(331) was regenerated at 72 h when deactivation was observed. Clearly, the conversion of AcOH reached 100% after regeneration, which indicates CZA(331) is highly stable and the deposited carbon can be completely removed under current regeneration conditions.

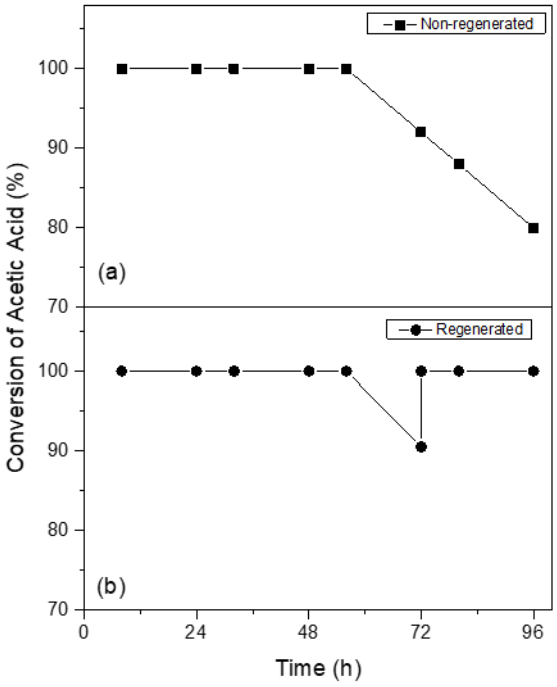

Figure 7. Conversion of acetic acid on (a) fresh CZA(331), (b) regenerated CZA(331) at 425 ºC.

4 Conclusion

$Ca/Zn/AlO_x$ mixed oxides (CZA) with various Ca/Zn/Al ratios resulted in the formation of various fractions of nano-sized CaO, ZnO, $ZnAl_2O_4$, amorphous alumina and calcium aluminates in catalysts. The crystallinity of CZA catalysts increased at higher Zn content, while increasing Al content promotes the formation of amorphous calcium aluminates. CZA catalysts with high Al content (> 1/3) provide mainly moderate basicity, which strongly increased from weak to strong with increasing (Ca+Zn) content as revealed by$TDP\text{-}CO_2$ studies.

In the ketonization of acetic acid, all CZA catalysts are highly active for AcOH conversion (93-100 %) at 425 ^oC with a selectivity of 97.1-100 % to acetone as a desired product. The performance of CZA catalysts strongly depends on their compositions and surface structure, and two reaction pathway are revealed. The strong basic sites (CaO and ZnO) on CZA catalysts with high (Ca+Zn) content governs the reaction at $T \geq 375$ ^oC. The acetates formed on these strong basic sites can be thermally decomposed to acetone and promoted at high temperature. CZA catalysts having high Al content are active at $T \leq 350$ ^oC. Increasing Al content can promote the formation of amorphous calcium aluminates, which helped the catalysts to provide acid-base pair sites, such as Al_2O_3 and CaO in proximity. Ketonization can be carried out over these acid-base pairs through acetone

enolized on basic sites (CaO), followed by nucleophilic attack of another AcOH adsorbed on neighboring Lewis acid sites (Al_2O_3) to form β-ketoacid as an intermediate, readily for decomposition into acetone and CO_2.

Among CZA catalysts, CZA(331) obtained the highest acetone yield of 97.1 % at 425 ^oC and exhibited stronger tolerance with furfural and phenol (major compounds in pyrolysis bio-oil) addition than CeO_2/Al_2O_3, reported as the most active oxides for ketonization earlier [7]. Moreover, CZA catalysts can perform the reaction for 56 h without any activity loss and be regenerated to recover full conversion of AcOH at 425 ^oC. This demonstrates CZA catalysts introduced here is very active, stable, high tolerance and easily to be regenerated, which is promising for industrial ketonization and bio-oil upgrading in future.

Acknowledgement

This work was supported by the Australian Research Council Discovery Projects (DP150103842 and DP140102432), the Faculty's MCR Scheme, Energy and Materials Clusters and the Early Career Research Scheme and the Major Equipment Scheme from the University of Sydney.

Reference

[1] T.N. Pham, T. Sooknoi, S.P. Crossley, D.E. Resasco, *Ketonization of carboxylic acids: mechanisms, catalysts, and implications for biomass conversion,* ACS Catal. **3** (2013) 2456-2473.

[2] G.W. Huber, S. Iborra, A. Corma, Synthesis of transportation fuels from biomass: Chemistry, catalysts, and engineering, Chem. Rev. 106 (2006) 4044-4098.

[3] R. Hilten, J. Weber, J.R. Kastner, Continuous upgrading of fast pyrolysis oil by simultaneous esterification and hydrogenation, Energy & Fuels 30 (2016) 8357-8368.

[4] T.P. Vispute, H.Y. Zhang, A. Sanna, R. Xiao, G.W. Huber, Renewable chemical commodity feedstocks from integrated catalytic processing of pyrolysis oils, Science 330 (2010) 1222-1227.

[5] J.P. Diebold, S. Czernik, Additives to lower and stabilize the viscosity of pyrolysis oils during storage, Energy & Fuels 11 (1997) 1081-1091.

[6] R. Aguado, M. Olazar, M.J.S. Jose, G. Aguirre, J. Bilbao, Pyrolysis of sawdust in a conical spouted bed reactor. Yields and product composition, Ind. & Eng. Chem. Res. 39 (2000) 1925-1933.

[7] L. Deng, Y. Fu, Q.-X. Guo, Upgraded acidic components of bio-oil through catalytic ketonic condensation, Energy & Fuels 23 (2009) 564-568.

[8] D.C. Elliott, Historical developments in hydroprocessing bio-oils, Energy & Fuels 21 (2007) 1792-1815.

[9] A.G. Gayubo, A.T. Aguayo, A. Atutxa, R. Aguado, J. Bilbao, Transformation of oxygenate components of biomass pyrolysis oil on a HZSM-5 zeolite. I.

Alcohols and phenols, Ind. & Eng. Chem. Res. 43 (2004) 2610-2618.

[10] A.G. Gayubo, A.T. Aguayo, A. Atutxa, R. Aguado, M. Olazar, J. Bilbao, Transformation of oxygenate components of biomass pyrolysis oil on a HZSM-5 zeolite. H. Aldehydes, ketones, and acids, Ind. & Eng. Chem. Res. 43 (2004) 2619-2626.

[11] Q. Zhang, J. Chang, T. Wang, Y. Xu, Upgrading bio-oil over different solid catalysts, Energy & Fuels 20 (2006) 2717-2720.

[12] C. Zhao, J.A. Lercher, Upgrading pyrolysis oil over Ni/HZSM-5 by cascade reactions, Angew. Chem. Int. Ed. 51 (2012) 5935-5940.

[13] G.W. Huber, I. S., C. A., Synthesis of Transportation fuels from biomass: chemistry, catalysts, and engineering, Chem. Rev. 106 (2006) 4044-4098.

[14] W.-J. Liu, X.-S. Zhang, Y.-C. Qv, H. Jiang, H.-Q. Yu, Bio-oil upgrading at ambient pressure and temperature using zero valent metals, Green Chem. 14 (2012) 2226-2233.

[15] A. Oasmaa, S. Czernik, Fuel oil quality of biomass pyrolysis oils - State of the art for the end user, Energy & Fuels 13 (1999) 914-921.

[16] R.W. Snell, S.H. Hakim, J.A. Dumesic, B.H. Shanks, Catalysis with ceria nanocrystals: Bio-oil model compound ketonization, Appl. Catal. A- Gen. 464–465 (2013) 288-295.

[17] G.A.H. Mekhemer, S.A. Halawy, M.A. Mohamed, M.I. Zaki, Ketonization of acetic acid vapour over polycrystalline magnesia: in situ Fourier transform infrared spectroscopy and kinetic studies, J. Catal. 230 (2005) 109-122.

[18] M. Renz, Ketonization of carboxylic acids by decarboxylation: mechanism and scope, Eur. J. Org. Chem. (2005) 979-988.

[19] T.N. Pham, D.C. Shi, D.E. Resasco, Evaluating strategies for catalytic

upgrading of pyrolysis oil in liquid phase, Appl. Catal. B-Environ. 145 (2014) 10-23.

[20] S.D. Randery, J.S. Warren, K.M. Dooley, Cerium oxide-based catalysts for production of ketones by acid condensation, Appl. Catal. A-Gen. 226 (2002) 265-280.

[21] M. Glinski, J. Kijenski, A. Jakubowski, Ketones from monocarboxylic acids - catalytic ketonization over oxide systems, Appl. Catal. A-Gen. 128 (1995) 209-217.

[22] O. Nagashima, S. Sato, R. Takahashi, T. Sodesawa, Ketonization of carboxylic acids over CeO_2-based composite oxides, J. Mol. Catal. A-Chem. 227 (2005) 231-239.

[23] F. Gonzalez, G. Munuera, J.A. Prieto, Mechanism of ketonization of acetic-acid on anatase TiO_2 surfaces, J. Chem. Soc. Faraday Trans. I 74 (1978) 1517-1529.

[24] T.N. Pham, D.C. Shi, T. Sooknoi, D.E. Resasco, Aqueous-phase ketonization of acetic acid over Ru/TiO_2/carbon catalysts, J. Catal. 295 (2012) 169-178.

[25] J.C. Kuriacose, S.S. Jewur, Studies on surface interaction of acetic-acid on iron-oxide, J. Catal. 50 (1977) 330-341.

[26] D. Mohan, C.U. Pittman, Jr., P.H. Steele, Pyrolysis of wood/biomass for bio-oil: A critical review, Energy & Fuels 20 (2006) 848-889.

[27] B. Sukhbaatar, P.H. Steele, L.L. Ingram, M.G. Kim, An exploratory study on the removal of acetic and formic acids from bio-oil, Bioresources 4 (2009) 1319-1329.

[28] K. Parida, J. Das, Mg/Al hydrotalcites: preparation, characterisation and

ketonisation of acetic acid, J. Mol. Catal. A-Chem. 151 (2000) 185-192.

[29] J. Das, K. Parida, Catalytic Ketonization of acetic acid on Zn/Al layered double hydroxides, Reaction Kinetics & Catal. Lette. 69 (2000) 223-229.

[30] D.E. Resasco, B. Wang, S. Crossley, Zeolite-catalysed C-C bond forming reactions for biomass conversion to fuels and chemicals, Catal. Sci. & Techn. 6 (2016) 2543-2559.

[31] A. Gumidyala, T. Sooknoi, S. Crossley, Selective ketonization of acetic acid over HZSM-5: The importance of acyl species and the influence of water, J. Catal. 340 (2016) 76-84.

[32] G. Busca, Acid catalysts in industrial hydrocarbon chemistry, Chem. Rev. 107 (2007) 5366-5410.

[33] C. Friedel, Ueber s. g. gemischte Acetone, Eur. J. Org. Chem. 108 (1858) 122-125.

[34] R. Pestman, R.M. Koster, A. vanDuijne, J.A.Z. Pieterse, V. Ponec, Reactions of carboxylic acids on oxides .2. Bimolecular reaction of aliphatic acids to ketones, J. Catal. 168 (1997) 265-272.

[35] A. Altay, C.B. Carter, I. Arslan, M.A. Gülgün, Crystallization of $CaAl_4O_7$ and $CaAl_{12}O_{19}$ powders, Philosophical Magaz. 89 (2009) 605-621.

[36] R. Pandey, J.D. Gale, S.K. Sampath, J.M. Recio, Atomistic simulation study of spinel oxides: Zinc aluminate and zinc gallate, J. Am. Ceramic Soc. 82 (1999) 3337-3341.

[37] W. Staszak, M. Zawadzki, J. Okal, Solvothermal synthesis and characterization of nanosized zinc aluminate spinel used in isobutane combustion, J. Alloys and Compounds 492 (2010) 500-507.

[38] X. Zhao, L. Wang, X. Xu, X. Lei, S. Xu, F. Zhang, Fabrication and

photocatalytic properties of novel ZnO/$ZnAl_2O_4$ nanocomposite with $ZnAl_2O_4$ dispersed inside ZnO network, AICHE J. 58 (2012) 573-582.

[39] B. Zhang, M. von Kcitz, K. Valentas, Maximizing the liquid fuel yield in a biorefining process, Biotechn. and Bioeng.101 (2008) 903-912.

[40] Y.H. Taufiq-Yap, H.V. Lee, M.Z. Hussein, R. Yunus, Calcium-based mixed oxide catalysts for methanolysis of Jatropha curcas oil to biodiesel, Biomass & Bioenergy 35 (2011) 827-834.

[41] S. Talam, S.R. Karumuri, N. Gunnam, Synthesis, characterization, and spectroscopic properties of ZnO nanoparticles, ISRN Nanotechn. 2012 (2012) 6.

[42] V. Ciupina, I. Carazeanu, G. Prodan, Characterization of $ZnAl_2O_4$ nanocrystals prepared by coprecipitation and microemulsion techniques, J. Optoelectronics and Adv. Mater. 6 (2004) 1317-1322.

[43] C. Ngamcharussrivichai, P. Totarat, K. Bunyakiat, Ca and Zn mixed oxide as a heterogeneous base catalyst for transesterification of palm kernel oil, Appl. Catal. A-Gen. 341 (2008) 77-85.

[44] M.I. Zaki, H. Knoezinger, B. Tesche, G.A.H. Mekhemer, Influence of phosphonation and phosphation on surface acid-base and morphological properties of CaO as investigated by in situ FTIR spectroscopy and electron microscopy, J. Colloid and Interf. Sci. 303 (2006) 9-17.

[45] A.W. Burton, K. Ong, T. Rea, I.Y. Chan, On the estimation of average crystallite size of zeolites from the Scherrer equation: A critical evaluation of its application to zeolites with one-dimensional pore systems, Microporous Mesoporous Mater. 117 (2009) 75-90.

[46] M. Broda, A.M. Kierzkowska, D. Baudouin, Q. Imtiaz, C. Copéret, C.R.

Müller, Sorbent-enhanced methane reforming over a Ni–Ca-based, bifunctional catalyst sorbent, ACS Catal. 2 (2012) 1635-1646.

[47] K.M. Jasim, F.A. Hashim, R.H. Yousif, R.D. Rawlings, A.R. Boccaccini, Actively brazed alumina to alumina joints using CuTi, CuZr and eutectic AgCuTi filler alloys, Ceramics Int. 36 (2010) 2287-2295.

[48] S. Ito, N. Umehara, H. Takata, T. Fujii, Phase transition of γ-Al_2O_3 under hot isostatic pressure, Solid State Ionics 172 (2004) 403-406.

[49] S. Wei, H. Cui, J. Wang, S. Zhuo, W. Yi, L. Wang, Z. Li, Preparation and activity evaluation of NiMoB/γ-Al_2O_3 catalyst by liquid-phase furfural hydrogenation, Particuology 9 (2011) 69-74.

[50] I. Maghsoudi, M.J. Hadianfard, H. Shokrollahi, The influence of Al content and CaO–SiO_2 on the magnetic and structural properties of Al-substituted Ni ferrites, J. Alloys and Compounds 481 (2009) 539-542.

[51] A.C. Alba-Rubio, J. Santamaría-González, J.M. Mérida-Robles, R. Moreno-Tost, D. Martín-Alonso, A. Jiménez-López, P. Maireles-Torres, Heterogeneous transesterification processes by using CaO supported on zinc oxide as basic catalysts, Catal. Today 149 (2010) 281-287.

[52] T.K. Parya, R.K. Bhattacharyya, S. Banerjee, U.B. Adhikari, Co-precipitated $ZnAl_2O_4$ spinel precursor as potential sintering aid for pure alumina system, Ceramics Int. 36 (2010) 1211-1215.

[53] D. Carriazo, M. del Arco, E. Garcia-Lopez, G. Marci, C. Martin, L. Palmisano, V. Rives, Zn,Al hydrotalcites calcined at different temperatures: Preparation, characterization and photocatalytic activity in gas-solid regime, J. Mol. Catal. A-Chem. 342-43 (2011) 83-90.

[54] M. Behrens, I. Kasatkin, S. Kuehl, G. Weinberg, Phase-pure Cu,Zn,Al

hydrotalcite-like materials as precursors for copper rich Cu/ZnO/Al_2O_3 catalysts, Chem. Mater. 22 (2010) 386-397.

[55] A.A. Voevodin, J.S. Zabinski, Nanocomposite and nanostructured tribological materials for space applications, Composites Sci. and Techn. 65 (2005) 741-748.

[56] J. Yu, F. Wang, Y. Wang, H. Gao, J. Li, K. Wu, Interfacial reaction growth approach to preparing patterned nanomaterials and beyond, Chem. Soc. Rev. 39 (2010) 1513-1525.

[57] D. Gouvêa, S.V. Ushakov, A. Navrotsky, Energetics of CO_2 and H_2O adsorption on zinc oxide, Langmuir 30 (2014) 9091-9097.

[58] Q. Liu, L. Wang, C. Wang, W. Qu, Z. Tian, H. Ma, D. Wang, B. Wang, Z. Xu, The effect of lanthanum doping on activity of Zn-Al spinel for transesterification, Appl. Catal. B-Environ.136–137 (2013) 210-217.

[59] T.R. Mandlimath, K.I. Sathiyanarayanan, Facile synthesis of $ZnAl_2O_4$ nanoparticles: efficient and reusable porous nano $ZnAl_2O_4$ and copper supported on $ZnAl_2O_4$ catalysts for one pot green synthesis of propargylamines and imidazo[1,2-a]pyridines by A3 coupling reactions, RSC Adv. 6 (2016) 3117-3125.

[60] P. Kumar, V.C. Srivastava, I.M. Mishra, Dimethyl carbonate synthesis from propylene carbonate with methanol using Cu-Zn-Al catalyst, Energy & Fuels 29 (2015) 2664-2675.

[61] S.S. Zumdahl, Chemical Principles 6th Ed., Houghton Mifflin Company. 2009.

[62] L. Bencivenni, S.C. Losada, A. Pieretti, J.J. Quirante, The bimolecular pyrolysis of acetic acid: an ab initio study, Chem. Phys. Lett. 276 (1997) 26-

30.

[63] H. Zou, J.Y. Shen, Microcalorimetric and infrared spectroscopic studies of gamma-Al_2O_3 modified by zinc oxide, Thermochimica Acta 351 (2000) 165-170.

[64] Y. Yamada, M. Segawa, F. Sato, T. Kojima, S. Sato, Catalytic performance of rare earth oxides in ketonization of acetic acid, J. Mol. Catal. A-Chem. 346 (2011) 79-86.

[65] L. Bencivenni, S.C. Losada, A. Pieretti, J.J. Quirante, The bimolecular pyrolysis of acetic acid: an ab initio study, Chem. Phys. Lett. 276 (1997) 26-30.

[66] K.J. Laidler, Chemical Kinetics, Third Edition, Harper & Row, 1987, 42.

[67] R.W. Snell, B.H. Shanks, Insights into the ceria-catalyzed ketonization reaction for biofuels applications, ACS Catal. 3 (2013) 783-789.

[68] M. Fleisher, V. Stonkus, I. Liepina, K. Edolfa, Theoretical study of the ketonization reaction mechanism of acetic acid over SiO_2, 13th International Electronic Conference on Synthetic Organic Chemistry, (2009).

[69] M.A. Hasan, M.I. Zaki, L. Pasupulety, Oxide-catalyzed conversion of acetic acid into acetone: an FTIR spectroscopic investigation, Appl. Catal. A-Gen. 243 (2003) 81-92.

[70] C. Martin, I. Martin, V. Rives, An FT-IR study of the adsorption of pyridine, formic-acid and acetic-acid on magnesia and molybdena magnesia, J. Mol. Catal. 73 (1992) 51-63.

[71] A.V. Ignatchenko, Density functional theory study of carboxylic acids adsorption and enolization on monoclinic zirconia surfaces, J. Phys. Chem. C 115 (2011) 16012-16018.

[72] A.V. Bridgwater, Principles and practice of biomass fast pyrolysis processes for liquids, J. Analyt. Appl. Pyrol. 51 (1999) 3-22.

[73] T.N. Pham, D. Shi, D.E. Resasco, Evaluating strategies for catalytic upgrading of pyrolysis oil in liquid phase, Appl. Catal. B-Environ.145 (2014) 10-23.

TOC

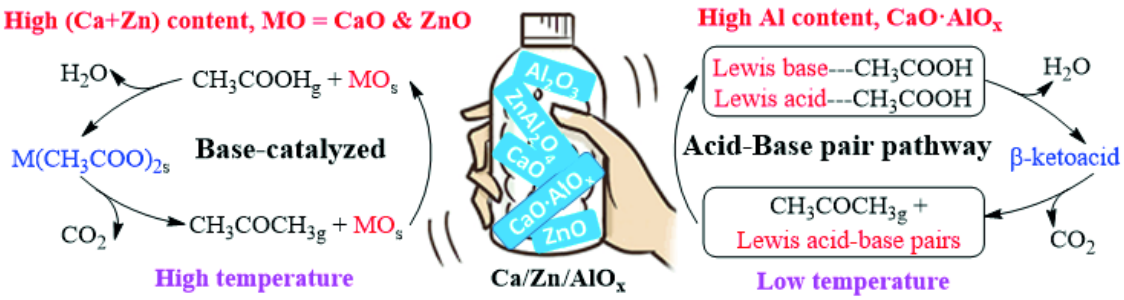
High (Ca+Zn) content, MO = CaO & ZnO
H2O
CH3COOHg + MOs
M(CH3COO)2s
Base-catalyzed
CO2
CH3COCH3g + MOs
High temperature
Al2O3
ZnAl2O4
CaO
CaO·AlOx
ZnO
Ca/Zn/AlOx
High Al content, CaO·AlOx
Lewis base---CH3COOH
Lewis acid---CH3COOH
Acid-Base pair pathway
H2O
β-ketoacid
CH3COCH3g +
Lewis acid-base pairs
CO2
Low temperature